Mechanism-Based Covalent Neuraminidase Inhibitors with Broad-Spectrum Influenza Antiviral Activity

Jin-Hyo Kim *et al.*

Science **340**, 71 (2013);
DOI: 10.1126/science.1232552

mean survival of recruits (<5 cm; $n = 1281$) of branching (*Acropora*) and massive (*Goniastrea*) corals during the recovery period (*13*) ranged from 83 to 93% each year (fig. S4), which is far higher than the <50% survival of recruits on reefs experiencing chronic pressures (*28*, *29*). Indeed, the mean survival of all ($n = 5333$) colonies was consistently higher than 80% each year, apart from the lower survival (>53% year^{-1}) of some larger (>15 cm) branching corals at sites exposed to cyclonic waves in 2007 (fig. S4). High survival and growth resulted in rapid rates of transition through increasing colony size classes, with corresponding increases in brood stock and reproductive output (*13*) (Fig. 3). Reproductive output and recruitment were similar to predisturbance levels within a decade of the bleaching, and 2 years later, coral cover and community structure had also recovered.

The recovery of corals at Scott Reef after the 1998 mass bleaching may have been even faster if not for a series of more moderate disturbances, including two cyclones, an outbreak of disease, and a second bleaching. This demonstrates that even coral reefs with a negligible supply of larvae from outside can recover relatively quickly from disturbances in the absence of chronic human pressures. Other ecosystems have displayed a similar resilience when environmental conditions were not fundamentally altered by human activities (*30*). Our results suggest that addressing local pressures, such as pollution and overfishing, is as important to the recovery of coral reefs as the establishment of networks of marine protected areas (MPAs). Managing local pressures to promote resilience will be critical to preventing the global degradation of coral reefs, with climate change likely to cause additional severe disturbances in the near future.

References and Notes

1. J. H. Connell, *Coral Reefs* **16** (suppl.), S101 (1997).
2. T. J. Done *et al*., *Coral Reefs* **26**, 789 (2007).
3. J. F. Bruno, E. R. Selig, *PLoS ONE* **2**, e711 (2007).
4. C. R. Wilkinson, Ed., *Status of Coral Reefs of the World* (Global Coral Reef Monitoring Network and Reef and Rainforest Research Centre, Townsville, Queensland, 2008).
5. R. van Woesik, *Biodivers. Conserv.* **9**, 1219 (2000).
6. G. De'ath, K. Fabricius, *Ecol. Appl.* **20**, 840 (2010).
7. T. J. Done, *Hydrobiologia* **247**, 121 (1992).
8. D. R. Bellwood, T. P. Hughes, C. Folke, M. Nyström, *Nature* **429**, 827 (2004).
9. T. P. Hughes, N. A. J. Graham, J. B. C. Jackson, P. J. Mumby, R. S. Steneck, *Trends Ecol. Evol.* **25**, 633 (2010).
10. R. K. Pachauri, A. Reisinger, Eds., *Climate Change 2007: Synthesis Report. Contribution of Working Groups I, II and III to the Fourth Assessment Report of the Intergovernmental Panel on Climate Change* (IPCC, Geneva, 2007).
11. A. J. Richardson, E. S. Poloczanska, *Science* **320**, 1294 (2008).
12. N. Knowlton, J. B. C. Jackson, *PLoS Biol.* **6**, e54 (2008).
13. See supplementary materials on *Science* Online.
14. C. R. Wilkinson, Ed., *Status of Coral Reefs of the World* (Australian Institute of Marine Science, Townsville, Queensland, 2004).
15. C. M. Roberts, *Science* **278**, 1454 (1997).
16. D. J. Ayre, T. P. Hughes, *Ecol. Lett.* **7**, 273 (2004).
17. N. A. J. Graham *et al*., *Proc. Natl. Acad. Sci. U.S.A.* **103**, 8425 (2006).
18. T. R. McClanahan *et al*., *PLoS ONE* **7**, e42884 (2012).
19. C. R. Wilkinson, Ed., *Status of Coral Reefs of the World* (Australian Institute of Marine Science, Townsville, Queensland, 2000).
20. NOAA, Coral Reef Watch: Coral Bleaching Virtual Stations (2013), http://coralreefwatch.noaa.gov/satellite/current/products_vs.html.
21. C. N. Mundy, *Coral Reefs* **19**, 124 (2000).
22. J. Gilmour, L. D. Smith, R. M. M. Brinkman, *Mar. Biol.* **156**, 1297 (2009).
23. J. N. Underwood, L. D. Smith, M. J. H. van Oppen, J. P. Gilmour, *Ecol. Appl.* **19**, 18 (2009).
24. R. B. Aronson, W. F. Precht, I. G. Macintyre, T. J. T. Murdoch, *Nature* **405**, 36 (2000).
25. G. Roff, P. J. Mumby, *Trends Ecol. Evol.* **27**, 404 (2012).
26. M. S. Pratchett *et al*., *Oceanogr. Mar. Biol. Annu. Rev.* **46**, 251 (2008).
27. P. J. Mumby, R. S. Steneck, *Trends Ecol. Evol.* **23**, 555 (2008).
28. M. Wittenberg, W. Hunte, *Mar. Biol.* **112**, 131 (1992).
29. T. P. Hughes, J. E. Tanner, *Ecology* **81**, 2250 (2000).
30. H. K. Lotze, M. Coll, A. M. Magera, C. Ward-Paige, L. Airoldi, *Trends Ecol. Evol.* **26**, 595 (2011).

Acknowledgments: The field work at Scott Reef was supported by crews of the AIMS Research Vessels Lady Basten, Cape Ferguson, and Solander. We thank K. Brooks, M. Case, J. Colquhoun, K. Cook, D. Ceccarelli, A. Cheal, J. Eagle, K. Fitzgerald, E. Gates, A. Halford, O. Hunt, D. Hoey, K. Markey, D. McKinney, S. Neale, R. Ninio, B. Radford, M. Rees, G. Suosaari, A. Thompson, M. Travers, and J. Underwood for help with data collection or analyses; J. Lough for help with sea surface temperature data; and K. Cook, A. McNeil, J. Oliver, and three anonymous reviewers for their comments. This research was jointly supported by the Australian Federal Government through the Australian Institute of Marine Science and the Browse LNG Development Joint Venture Participants, through the operator Woodside Energy Limited. J.P.G., L.D.S., and A.J.H. designed the experiments and collected and managed the data. J.P.G., L.D.S., A.H.B., and M.S.P. analyzed and interpreted the data, and all authors wrote the paper. Data used in this paper can be accessed at the AIMS Data Catalogue at http://data.aims.gov.au/metadataviewer/uuid/efc0b6f4-1eb1-48f0-8673-b161d68f0f2f.

Supplementary Materials

www.sciencemag.org/cgi/content/full/340/6128/69/DC1
Materials and Methods
Figs. S1 to S4
Table S1
References (*31*–*40*)

2 November 2012; accepted 20 February 2013
10.1126/science.1232310

Mechanism-Based Covalent Neuraminidase Inhibitors with Broad-Spectrum Influenza Antiviral Activity

Jin-Hyo Kim,[1]*† Ricardo Resende,[1]* Tom Wennekes,[1]*‡ Hong-Ming Chen,[1]* Nicole Bance,[2] Sabrina Buchini,[1]§ Andrew G. Watts,[3] Pat Pilling,[4] Victor A. Streltsov,[4] Martin Petric,[5] Richard Liggins,[6] Susan Barrett,[4] Jennifer L. McKimm-Breschkin,[4] Masahiro Niikura,[2] Stephen G. Withers[1]||

Influenza antiviral agents play important roles in modulating disease severity and in controlling pandemics while vaccines are prepared, but the development of resistance to agents like the commonly used neuraminidase inhibitor oseltamivir may limit their future utility. We report here on a new class of specific, mechanism-based anti-influenza drugs that function through the formation of a stabilized covalent intermediate in the influenza neuraminidase enzyme, and we confirm this mode of action with structural and mechanistic studies. These compounds function in cell-based assays and in animal models, with efficacies comparable to that of the neuraminidase inhibitor zanamivir and with broad-spectrum activity against drug-resistant strains in vitro. The similarity of their structure to that of the natural substrate and their mechanism-based design make these attractive antiviral candidates.

The envelope of the influenza virus contains two immunodominant glycoproteins, hemagglutinin (HA) and neuraminidase (NA), that play key roles in viral infection and spread. HA effects attachment of the virus to the host cell through its interaction with surface sialic acids, thereby initiating entry. Once the virus has replicated, the NA cleaves sialic acids from the viral and cell surfaces, allowing the virus progeny to spread to uninfected cells. On the basis of the notion that potent and specific viral NA inhibitors should function to reduce viral spread, structure-based inhibitor design programs have

[1]Department of Chemistry, University of British Columbia, 2036 Main Mall, Vancouver, British Columbia V6T 1Z1, Canada. [2]Faculty of Health Sciences, Simon Fraser University, 8888 University Drive, Burnaby, British Columbia V5A 1S6, Canada. [3]Department of Pharmacy and Pharmacology, University of Bath, Claverton Down, Bath BA27AY, UK. [4]Commonwealth Scientific and Industrial Research Organization, Materials Science and Engineering, 343 Royal Parade, Parkville 3052, Australia. [5]British Columbia Centre for Disease Control, Provincial Health Services Authority, Vancouver, British Columbia V5Z 4R4, Canada. [6]Centre for Drug Research and Development (CDRD), 2259 Lower Mall, Vancouver, British Columbia V6T 1Z4, Canada.

*These authors contributed equally to this work.
†Present address: Division of Chemical Safety, National Academy of Agricultural Science, RDA, 126 Suin-ro, Suwon 441-707, Republic of Korea.
‡Present address: Laboratory of Organic Chemistry, Wageningen University, Dreijenplein 8, 6703 HB Wageningen, Netherlands.
§Present address: Nano Bridging Molecules SARte Cité-Ouest 2,CH-1196 Gland, Switzerland.
||Corresponding author. E-mail: withers@chem.ubc.ca

produced two widely used anti-influenza drugs, zanamivir (Relenza) and oseltamivir (Tamiflu) (*1*) (Fig. 1A). These reversible inhibitors were designed to mimic the transition state, with a guanidinium or ammonium substituent added at the position corresponding to C-4 of the natural substrate to bind in an anionic pocket, thereby increasing affinity and specificity over human NAs. However, drug-resistant strains are now emerging, particularly against the more widely used and structurally divergent drug oseltamivir, highlighting an urgent need for new classes of NA inhibitors that differ minimally in structure from the parent sialic acid, given that the development of resistance to structurally conservative, mechanism-based inhibitors should be a much less probable event (*2*–*10*).

NAs catalyze the hydrolysis of sialosides with net retention of stereochemistry at the site of substitution. A mechanism involving an ion-pair intermediate has long been suggested for the GH34 (*11*) influenza NA (*12*), although involvement of a covalent intermediate, as has been shown for GH33 NAs (*13*), has emerged as an alternative. We provide evidence for such a covalent intermediate by use of 2,3-difluorosialic acid (**1**, DFSA) (Fig. 1B) as a substrate that exhibits slow turnover. The electronegative fluorine atom at C-3 inductively destabilizes the oxocarbenium ion-like transition states for both formation and hydrolysis of the intermediate, thus slowing each step, whereas the C-2 anomeric fluoride leaving group speeds the formation step, permitting accumulation of the covalent intermediate (Fig. 1B). Rapid inactivation of N9 NA was observed at low inactivator concentrations, such that individual kinetic parameters (K_i and k_i) could not be determined; only a second-order rate constant k_i/K_i of 196 min^{-1} mM^{-1} could be measured. Turnover of the covalent intermediate (k_{hydr}) also occurred rapidly, with a $t_{1/2} < 1$ min. Confirmation of the formation of a covalent species and identification of the site of attachment was achieved by peptic digestion of N9 NA that had been labeled with DFSA **1**, or by its difluoroKDN analog (figs. S1 to S3). Isolation and subsequent sequence analysis of the labeled peptide by liquid chromatography–based tandem mass spectrometry identified this peptide as NTDWSG**Y**SSSGSF, with the tyrosine (Y) bearing the sugar label, thereby confirming that Y406 functions as a catalytic nucleophile.

Knowing that the influenza NAs employ a covalent mechanism, we explored these DFSAs as a possible new class of covalent mechanism–based influenza therapeutics. These are attractive because the initial affinity of the drug (K_i) can be optimized, as well as the relative rate constants for formation (k_i) and hydrolysis (k_{hydr}) of the trapped intermediate, with the objective being to optimize the ratio of k_i/k_{hydr}. Versions of **1** bearing amine (Am) and guanidine (Gu) substituents at C-4 were of interest because these cationic substituents might improve the initial affinity and

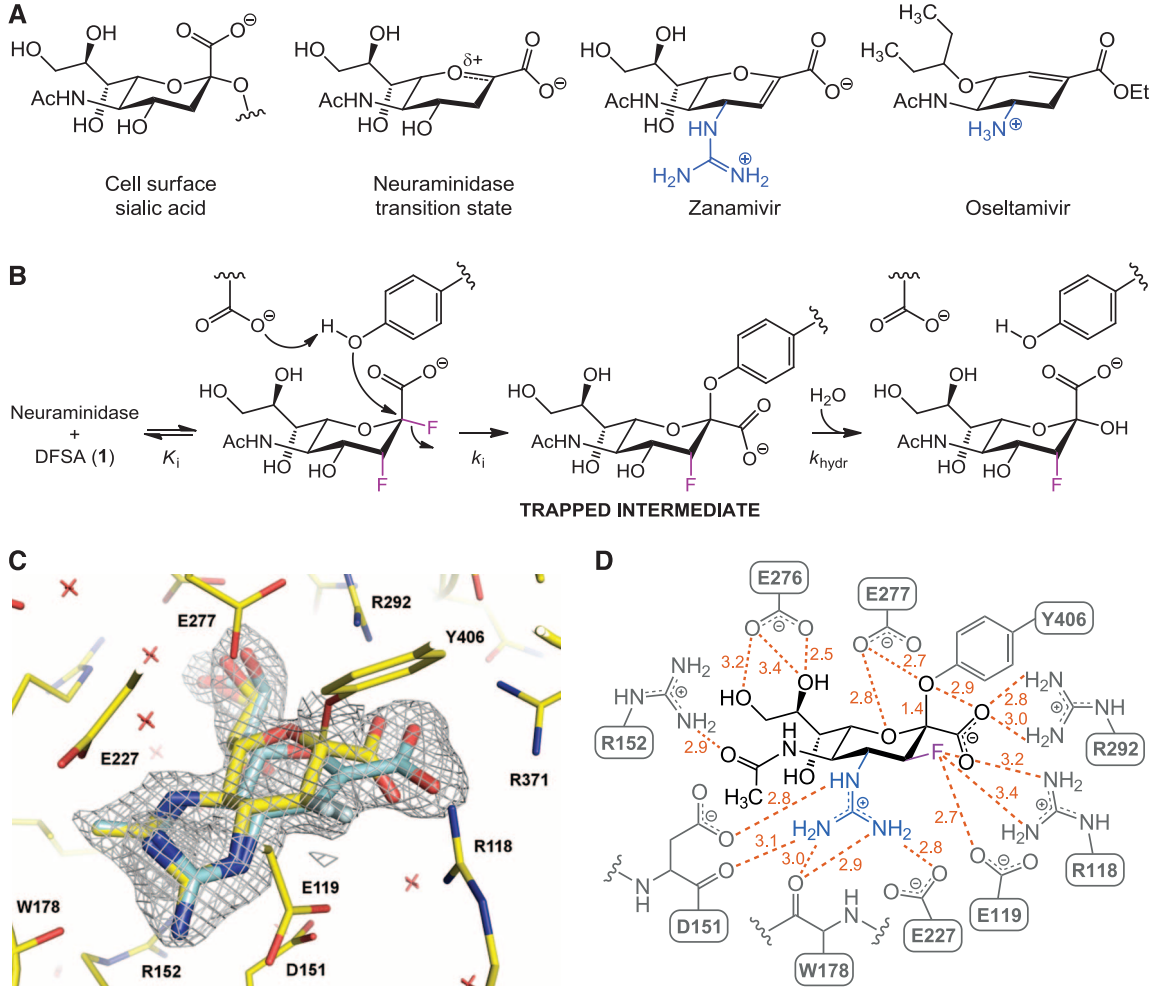

Fig. 1. Structures of key influenza therapeutics, mechanism of action of DFSAs, and x-ray structure of inhibited enzyme. (**A**) Chemical structures of cell surface sialic acids, the neuraminidase transition state, zanamivir (Relenza), and oseltamivir (Tamiflu). (**B**) Mechanism of action of the DFSAs. (**C**) X-ray crystallographic structure of the active site of the enzyme trapped as its 3-fluoro(eq)-4-guanidino-sialyl-enzyme intermediate (elimination product is in pale cyan) overlaid with omit (*22*) electron density map shown as a gray mesh contoured at 1σ within 1.6 Å of ligands. The electron density extends from the ligand molecule to Y406, suggesting a covalent link between the inhibitor's C-2 atom and the OH of Y406. (**D**) Diagram of interactions (orange dashed lines; distances in Å) with the sialic acid in the covalently inhibited enzyme. The corresponding diagram of interactions for the elimination product is shown in fig. S4.

Table 1. Inactivation and reactivation parameters for difluorosialic acids (DFSAs).*

Compound	Virus†	k_i/K_i ($min^{-1}mM^{-1}$)	$t_{1/2\ (inac)}$ (min)	$t_{1/2\ (reac)}$ (min)
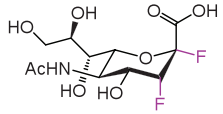 DFSA (**1**)	G70C H1N9	196	N.D.‡	< 1
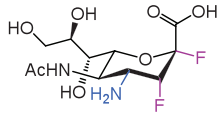 FaxAmDFSA (**2**)	Brisbane H1N1	106	2.1	6900
	Brisbane H1N1 H275Y	29	2.5	3450
	California H1N1	95	1.7	6900
	G70C H1N9	74	4.0	2300
	Hong Kong H3N2	140	20.8	>6900
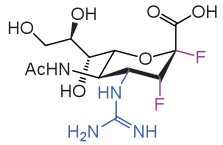 FaxGuDFSA (**3**)	Brisbane H1N1	371	7.4	>6900
	Brisbane H1N1 H275Y	160	9.2	>6900
	California H1N1	93	20.9	>6900
	G70C H1N9	246	6.8	>6900
	Hong Kong H3N2	470	20.2	>6900
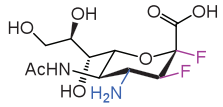 FeqAmDFSA (**4**)	Brisbane H1N1	3479	0.9	256
	Brisbane H1N1 H275Y	849	0.2	117
	California H1N1	4422	0.4	46
	G70C H1N9	4332	0.8	49
	Hong Kong H3N2	5662	---	153
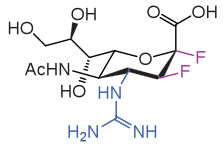 FeqGuDFSA (**5**)	Brisbane H1N1	5812	0.3	1380
	Brisbane H1N1 H275Y	2992	0.5	460
	California H1N1	7594	0.9	690
	G70C H1N9	3879	0.5	363
	Hong Kong H3N2	5737	0.8	1380

*Refer to table S4 for full kinetic parameters. †Brisbane H1N1, A/Brisbane/59/07; Brisbane H1N1 H275Y, A/Brisbane/59/07 oseltamivir-resistant; California H1N1, A/California/07/09; G70C H1N9, A/NWS/G70C/75; Hong Kong H3N2, A/HongKong/01/68. ‡N.D., Not determined.

Table 2. IC_{50} values (nM) in the enzyme inhibition assay for wild-type and mutant pairs. Boldface indicates resistance to zanamivir or oseltamivir. IC_{50} is the concentration of inhibitor that reduces enzyme activity by 50% compared to the control uninhibited value. Values are the means of duplicate assays.

Virus*	Zanamivir	Oseltamivir	DFSA (1)	FaxAm DFSA (2)	FaxGu DFSA (3)	FeqAm DFSA (4)	FeqGu DFSA (5)
B/Perth	8.9	104.4	70	210	54	5.4	4.5
B/Perth D197E	**257.5**	**708.0**	170	340	162	16	8
A/Mississippi H1N1	1.9	3.1	80	840	115	45	13
A/Mississippi H1N1 H275Y	2.2	**2440**	120	2210	217	86	44
A/Fukui H3N2	3.8	1.7	1380	4710	2006	71	25
A/Fukui H3N2 E119V	3.4	**260.0**	240	2440	998	265	2.4
G70C H1N9	2.7	2.8	1190	2700	66.7	270	140
G70C H1N9 E119G	**678.4**	2.9	1150	1600	1433	73	17

*B/Perth, B/Perth/211/01; B/Perth D197E, B/Perth/211/01 zanamivir and oseltamivir-resistant; A/Mississippi H1N1, A/Mississippi/3/01; A/Mississippi H1N1 H275Y, A/Mississippi/3/01 oseltamivir-resistant; A/Fukui H3N2, A/Fukui/45/01; A/Fukui H3N2 E119V, A/Fukui/45/01 oseltamivir-resistant; G70C H1N9, A/NWS/G70C/75; G70C H1N9 E119G, A/NWS/G70C/75 zanamivir-resistant

the specificity for the influenza enzyme and also slow down the turnover of the intermediate, both through improved interactions of the intermediate species with the enzyme and by inductively destabilizing the reaction transition state. The effects of axial (ax) or equatorial (eq) stereochemistry of F3 on inhibitory behavior were also explored. Synthesis of the protected diastereomeric 3-axial and 3-equatorial-2,3-difluoro-4-azido neuraminic acids as key intermediates was achieved by Selectfluor hydroxyfluorination of 2,4-dideoxy-2,3-didehydro-4-azido-N-acetylneuraminic acid (4-azido-DANA) (*14*) followed by installation of an equatorial fluorine at C-2 using diethylaminosulfur trifluoride (DAST). The lead candidates shown in Table 1—FaxAmDFSA (**2**), FaxGuDFSA (**3**), FeqAmDFSA (**4**), and FeqGuDFSA (**5**)—were then prepared by reduction or reductive guanidylation, followed by deprotection (*15*).

Kinetic parameters for inactivation and reactivation of N1, N2, and N9 NAs, as representative influenza group 1 and group 2 enzymes, by **2** to **5** are presented in Table 1 and table S4, along with parameters for the parent DFSA **1** with the N9 NA. Not only did incorporation of the charged substituent at C-4 result in high initial affinity, but also, more importantly, it greatly reduced the rate constant for reactivation of enzymes inactivated by **2**, **3**, **4** and **5**, with half-lives for reactivation now ranging from 0.75 hours to >100 hours. The viral NA will therefore remain inactivated for extended times, even after the compound may have been cleared from relevant tissues, with favorable consequences for pharmacokinetic behavior. Interestingly, compounds with an equatorial fluorine at C-3 inactivated and reactivated faster than did those with an axial fluorine, typically by a factor of 10 to 40. Furthermore, a guanidine substituent at C-4 slowed both the inactivation and reactivation more than did an amine substituent, with a much greater effect on the reactivation step. This difference in rates likely has its origins in optimized interactions of the guanidine with the active site at the stage of the covalent intermediate, as is seen in the crystal structure of the trapped species shown in Fig. 1C. A covalent bond of 1.45 Å is observed in the electron density map (Fig. 1C and table S1), between C-2 of 3-fluoro (eq) sialic acid and the phenolic oxygen of Y406, and the C-4 guanidine indeed forms strong interactions with the anionic pocket, very similar to those found with zanamivir (*1*). As observed previously in a structure of the GH33 sialidase NanI (*16*), the covalent intermediate species is accompanied by an unsaturated form of fluorosialic acid formed by elimination.

An absolute comparison of the in vitro efficacy of these compounds as enzyme inhibitors with those of zanamivir or oseltamivir is difficult given their different modes of action, covalent versus noncovalent, and the time dependence of inhibition (*17*). However, a pragmatic measure was achieved by measuring median inhibitory concentration (IC_{50}) values for each DFSA, as well as zanamivir and oseltamivir carboxylate,

against four different virus strains and resistant mutants after preincubation for 30 min before substrate addition (Table 2). In almost all cases, each compound with an equatorial fluorine was a superior inhibitor to its axial epimer. Likewise, in each case the guanidine derivative showed superior performance to its amine analog. Consequently, compound **5** (FeqGuDFSA) was the optimal derivative, with IC_{50} values comparable to those for zanamivir and oseltamivir, "on rates" that are generally superior to those of zanamivir, and off rates that are lower (*1*, *18*, *19*).

The specificity of these inhibitors was then evaluated by testing them against Neu2 as a representative human NA (all human NAs belong to the sequence-related family GH33). No inactivation of Neu2 was seen with either of the amine derivatives. Inactivation by FaxGuDFSA (**3**) and FeqGuDFSA (**5**) occurred slowly, but at rates lower by a factor of 10^5 to 10^6 than those seen for inactivation of influenza NA at comparable concentrations. By comparison, zanamivir inhibits Neu2 with a K_i of 17 μM, a factor of only 10^3 to 10^4 higher than for influenza NA (*20*).

On the basis of these results, the ability of compounds **2** to **5** to inhibit the replication of the virus in cell culture was explored using MDCK cells (Madin-Darby canine kidney cells). Three A strains (N1, N2, and N9) plus one B strain were tested in plaque size reduction assays (PRA), with zanamivir as control. All DFSAs inhibited virus replication (Table 3 and figs. S5 to S8) with no cytotoxicity observed, even at 5 mM DFSA concentrations, as measured by neutral red staining of viable cells. For all strains, substitution with the 4-amino group enhanced inhibition of virus replication over the parent DFSA, and the 4-guanidino substitution was better still. Likewise the presence of an equatorial rather than axial fluorine in the 4-guanidino version resulted in a further 10-fold enhancement in potency for three of the strains tested. Consequently, FeqGuDFSA (**5**) had the highest potency of all of the inhibitors, including zanamivir, against the influenza B virus (fig. S5) and performed comparably against the influenza A strains. Importantly, the PRA data largely mirror the in vitro kinetic data, with the compounds possessing an equatorial fluorine being superior to those with an axial fluorine, and the 4-guanidino substitution being superior to a 4-amino. Furthermore, the absolute IC_{50} values in these PRAs were consistently lower than those for enzyme inhibition for all compounds except FeqAmDFSA (**4**) and in all cases were in the low nanomolar range. The DFSA derivatives also proved effective in vitro against NAs from a series of resistant strains, with FeqGuDFSA (**5**) again proving to be the most widely active (Table 2). All compounds proved effective against the oseltamivir-resistant H275Y mutant, wherein binding of the isopentyl side chain of oseltamivir is compromised. Importantly, the E119G mutation, which disrupts interactions with the 4- guanidine of zanamivir (reduction in efficacy by a factor of 250) (*5*) only reduced the efficacy of FaxGuDFSA (**3**) by a factor of 20. Notably, the efficacy of FeqGuDFSA (**5**) was enhanced by a factor of ~10 for the E119G- and oseltamivir-resistant E119V mutants. Selection against transition state analog binding (zanamivir) clearly does not equivalently suppress covalent intermediate accumulation. This excellent profile against otherwise resistant strains supports the concept of mechanism-based inhibition as a means to minimize selection of resistant strains.

Before commencing in vivo efficacy studies in mouse models, the pharmacokinetic properties of FaxGuDFSA (**3**) as a representative DFSA derivative were evaluated for administration by intravenous and intranasal routes and shown to be comparable to those collected in parallel for zanamivir, as shown in table S2. Efficacy tests were then conducted using a mouse-adapted influenza A virus strain, A/Hong Kong/1/68 (H3N2) (*21*). Balb/c mice were treated with either DFSA derivative, zanamivir, or saline twice daily by intranasal administration, starting 2 hours before infection. At a dose of 1 mg per kg of weight per day (mg/kg/day), FaxGuDFSA showed superior results to FaxAmDFSA in prolonging survival. At a higher dose of 10 mg/kg/day, it protected all the mice from the lethal infection, as did zanamivir (Fig. 2A). Measurement of viral RNA loads in lung tissue confirmed that survival was indeed associated with suppression of viral replication.

Table 3. IC_{50} values in the plaque size reduction assay. Values are the means of duplicate assays.

Virus*	Zanamivir	DFSA (1)	FaxAm DFSA (2)	FaxGu DFSA (3)	FeqAm DFSA (4)	FeqGu DFSA (5)
B/Perth	10 nM	1 μM	100 nM	10–100 nM	10–100 nM	1 nM
A/Mississippi H1N1	≤1 nM	1 μM	100 nM	10 nM	100 nM	1 nM
A/Fukui H3N2	100 nM	100 μM	1 μM	100 nM	1 μM	10 nM
G70C H1N9	1–10 nM	1–10 μM	1 μM	1–10 nM	1 μM	10 nM

*B/Perth, B/Perth/211/01; A/Mississippi H1N1, A/Mississippi/3/01; A/Fukui H3N2, A/Fukui/45/01; G70C H1N9, A/NWS/ G70C/75.

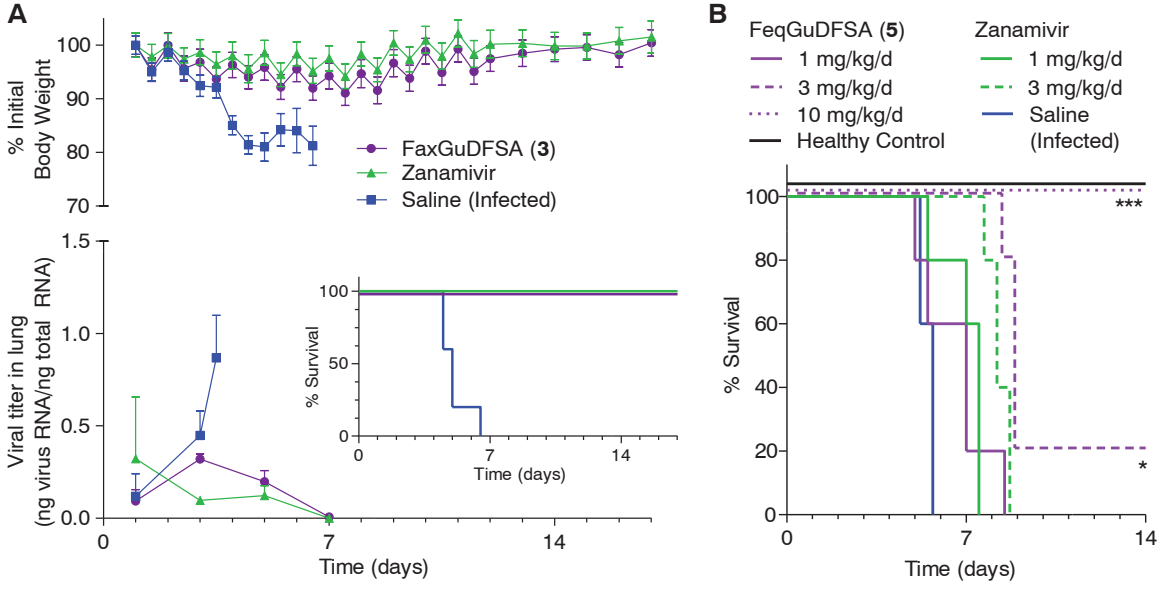

Fig. 2. Efficacy of FaxGuDFSA (3), FeqGuDFSA (5), and zanamivir in treating H3N2 influenza infection in the Balb/c mouse. (**A**) The top graph shows body weight over the 17-day observation period. Animals that lost 20% of initial weight were recorded as nonsurvivors, as indicated in the survival plot (inset). Ten animals per group were used for this experiment. In another set of animals, viral RNA loads were measured over 7 days by quantitative real-time fluorescence polymerase chain reaction (bottom graph). The entire lung tissue was collected from four animals at each time point for each treatment except for the last time point for the saline control. In this experiment, all saline control animals survived less than 4 days, and the last time point for this group shown is at 80 hours after infection (seven animals). (**B**) Dose-dependent efficacy of FeqGuDFSA (**5**) (1 to 10 mg/kg/day) and zanamivir. *Mantel Cox $P = 0.03$; ***Mantel Cox $P < 0.001$. Five animals per group were challenged and treated as indicated.

Likewise, dose dependency of FeqGuDFSA in the protection of mice was demonstrated with 100% efficacy at 10 mg/kg/day (Fig. 2B and table S3), with no ill effects in the treated animals during the experiments compared with the saline control.

The DFSAs represent a distinct class of potent, mechanism-based, specific NA inhibitor functioning by transient formation of a covalent intermediate species. Their high efficacy as enzyme inhibitors is matched by excellent antiviral activity in cell-based plaque size reduction assays, at levels similar or superior to those for zanamivir. Furthermore, they show good inhibition of NAs from zanamivir- or oseltamivir-resistant influenza virus strains, indicating an altered resistance profile. Most important, they function well in controlling influenza infections in an animal model, at levels comparable to those used for zanamivir.

References and Notes

1. M. von Itzstein *et al*., *Nature* **363**, 418 (1993).
2. J. L. McKimm-Breschkin *et al*., *J. Virol.* **72**, 2456 (1998).
3. M. Tashiro *et al*.; Neuraminidase Inhibitor Susceptibility Network, *Antivir. Ther.* **14**, 751 (2009).
4. M. Kiso *et al*., *Lancet* **364**, 759 (2004).
5. J. N. Varghese *et al*., *Structure* **6**, 735 (1998).
6. T. J. Blick *et al*., *Virology* **214**, 475 (1995).
7. L. V. Gubareva, M. J. Robinson, R. C. Bethell, R. G. Webster, *J. Virol.* **71**, 3385 (1997).
8. A. Eshaghi *et al*., *Emerg. Infect. Dis.* **17**, 1472 (2011).
9. H. T. Nguyen, A. M. Fry, P. A. Loveless, A. I. Klimov, L. V. Gubareva, *Clin. Infect. Dis.* **51**, 983 (2010).
10. E. van der Vries, F. F. Stelma, C. A. Boucher, *N. Engl. J. Med.* **363**, 1381 (2010).
11. The CAZY Glycoside Hydrolase (GH) database classifies carbohydrate-active enzymes on the basis of sequence similarities. Most bacterial and mammalian sialidases/neuraminidases belong to family GH33.
12. M. von Itzstein, *Nat. Rev. Drug Discov.* **6**, 967 (2007).
13. A. G. Watts *et al*., *J. Am. Chem. Soc.* **125**, 7532 (2003).
14. M. von Itzstein, B. Jin, W. Y. Wu, M. Chandler, *Carbohydr. Res.* **244**, 181 (1993).
15. See supplementary materials on *Science* Online for synthesis and characterization.
16. S. L. Newstead *et al*., *J. Biol. Chem.* **283**, 9080 (2008).
17. S. Barrett, P. G. Mohr, P. M. Schmidt, J. L. McKimm-Breschkin, *PLoS ONE* **6**, e23627 (2011).
18. P. J. Collins *et al*., *Nature* **453**, 1258 (2008).
19. E. van der Vries *et al*., *PLoS Pathog.* **8**, e1002914 (2012).
20. L. M. Chavas *et al*., *J. Med. Chem.* **53**, 2998 (2010).
21. E. G. Brown, H. Liu, L. C. Kit, S. Baird, M. Nesrallah, *Proc. Natl. Acad. Sci. U.S.A.* **98**, 6883 (2001).
22. M. D. Winn *et al*., *Acta Crystallogr. D Biol. Crystallogr.* **67**, 235 (2011).

Acknowledgments: We thank the Canadian Institutes for Health Research, the Pfizer CDRD Innovation Fund, the Canadian Foundation for Innovation, and the British Columbia Knowledge Development Fund for support of this work. S.G.W. is supported by a Tier 1 Canada Research Chair. J.-H.K. was supported by fellowships from the Korea Research Foundation (KRF-2005-214-C00215) and the Michael Smith Foundation for Health Research. T.W. was supported by the Netherlands Organization for Scientific Research (NWO) through a Rubicon fellowship. Parts of this work were funded by grant G0600514 from the Medical Research Council UK to A.G.W. and J.L.M.-B. and Pandemic influenza grant 595625 from the National Health and Medical Research Council Australia to J.L.M.-B. The authors acknowledge the use of the MX1 beamline at the Australian Synchrotron, Victoria, Australia. The data presented in this paper were tabulated in the main paper and the supplementary materials. Coordinates of the complex have been deposited in the Protein Data Bank with code 3W09. Patent protection for compounds described has been sought by the University of British Columbia under the following applications: PCT/CA2010/001063 "2,3-Fluorinated Glycosides as Neuraminidase Inhibitors and their Use as Anti-Virals" (S.G.W., A.G.W., J.-H.K., and T.W.); PCT/CA2013/050034 "3' Equatorial-Fluorine-Substituted Neuraminidase Inhibitor Compounds, Compositions and Methods for the Use Thereof as Anti-Virals" (S.G.W., H.-M.C., and R.R).

Supplementary Materials

www.sciencemag.org/cgi/content/full/science.1232552/DC1
Materials and Methods
Figs. S1 to S8
Tables S1 to S4
References (*23*–*43*)

9 November 2012; accepted 13 February 2013
Published online 21 February 2013;
10.1126/science.1232552

Decameric SelA•tRNA^{Sec} Ring Structure Reveals Mechanism of Bacterial Selenocysteine Formation

Yuzuru Itoh,[1,2,3] Markus J. Bröcker,[4] Shun-ichi Sekine,[1,2] Gifty Hammond,[4] Shiro Suetsugu,[3] Dieter Söll,[4,5]* Shigeyuki Yokoyama[1,2]*

The 21st amino acid, selenocysteine (Sec), is synthesized on its cognate transfer RNA (tRNA^{Sec}). In bacteria, SelA synthesizes Sec from Ser-tRNA^{Sec}, whereas in archaea and eukaryotes SepSecS forms Sec from phosphoserine (Sep) acylated to tRNA^{Sec}. We determined the crystal structures of *Aquifex aeolicus* SelA complexes, which revealed a ring-shaped homodecamer that binds 10 tRNA^{Sec} molecules, each interacting with four SelA subunits. The SelA N-terminal domain binds the tRNA^{Sec}-specific D-arm structure, thereby discriminating Ser-tRNA^{Sec} from Ser-tRNA^{Ser}. A large cleft is created between two subunits and accommodates the 3′-terminal region of Ser-tRNA^{Sec}. The SelA structures together with in vivo and in vitro enzyme assays show decamerization to be essential for SelA function. SelA catalyzes pyridoxal 5′-phosphate–dependent Sec formation involving Arg residues nonhomologous to those in SepSecS. Different protein architecture and substrate coordination of the bacterial enzyme provide structural evidence for independent evolution of the two Sec synthesis systems present in nature.

The micronutrient selenium is required for human and animal health (*1*). Selenium is present in proteins in the form of the 21st amino acid, selenocysteine (Sec), in which the thiol moiety of cysteine is replaced by a selenol group (*2*). Sec is located in the active sites of many redox enzymes and is encoded by a UGA stop codon in all three domains of life (*3*). Sec lacks its own aminoacyl-tRNA synthetase and is synthesized by the tRNA-dependent conversion of Ser (*3*). The first step in Sec synthesis is the formation of Ser-tRNA^{Sec} by seryl-tRNA synthetase (SerRS) (*3*). In bacteria, the selenocysteine synthase SelA then converts the Ser-tRNA^{Sec} to Sec-tRNA^{Sec}. Archaea and eukaryotes use an intermediate step in which the hydroxyl group of Ser-tRNA^{Sec} is phosphorylated by *O*-phosphoseryl-tRNA kinase (PSTK) (*4*) to give Sep-tRNA^{Sec}, the substrate for the homotetrameric enzyme SepSecS, the final synthetic enzyme (*5*, *6*). Both SelA and SepSecS are fold-type-I pyridoxal 5′-phosphate (PLP)–dependent enzymes (*7*) that use selenophosphate as the selenium donor (*3*, *8*). All Sec-synthesis systems must strictly discriminate Ser-tRNA^{Sec} from Ser-tRNA^{Ser}. tRNA^{Sec} is the longest tRNA (*9*), and its tertiary structure is quite different from that of a canonical tRNA (*8*, *10*). In archaea and eukaryotes, PSTK discriminates Ser-tRNA^{Sec} from Ser-tRNA^{Ser} for phosphorylation (*11*), and then SepSecS recognizes Sep-tRNA^{Sec} in a phosphate-dependent manner (*8*). However, because of the lack of crystallographic studies on SelA, the discrimination mechanism in bacteria has remained elusive. Cryogenic electron microscopy suggested SelA to be a homodecameric enzyme of >500 kD (*12*, *13*), in contrast to the ~220-kD SepSecS homotetramer (*8*).

Here, we present the crystal structures of full-length decameric *Aquifex aeolicus* SelA (SelA-FL, residues 1 to 452), alone (3.9 Å resolution) and in complex with *Thermoanaerobacter tengcongensis* tRNA^{Sec} (7.5 Å), and of a SelA mutant lacking the N-terminal domain (SelA-ΔN, residues 62 to 452) with and without thiosulfate (3.25 and 3.20 Å, respectively). Biochemical and genetic

[1]RIKEN Systems and Structural Biology Center, Tsurumi, Yokohama 230-0045, Japan. [2]Department of Biophysics and Biochemistry and Laboratory of Structural Biology, Graduate School of Science, The University of Tokyo, Bunkyo-ku, Tokyo 113-0033, Japan. [3]Laboratory of Membrane and Cytoskeleton Dynamics, Institute of Molecular and Cellular Biosciences, The University of Tokyo, Bunkyo-ku, Tokyo 113-0032, Japan. [4]Department of Molecular Biophysics and Biochemistry, Yale University, New Haven, CT 06520–8114, USA. [5]Department of Chemistry, Yale University, New Haven, CT 06520–8114, USA.

*Corresponding author. E-mail: dieter.soll@yale.edu (D.S.); yokoyama@riken.jp (S.Y.)